



Alteration of N⁶-Methyladenosine mRNA Methylation in a Human Stem Cell-Derived Cardiomyocyte Model of Tyrosine Kinase Inhibitor-Induced Cardiotoxicity

Yan Ma^{1†}, Xian Liu^{2†}, Yiming Bi¹, Tianhu Wang¹, Cheng Chen¹, Yabin Wang¹, Dong Han^{1*} and Feng Cao^{1*}

¹ National Clinical Research Center for Geriatric Diseases, The Second Medical Center, Chinese People's Liberation Army (PLA) General Hospital, Beijing, China, ² Department of Pharmaceutical Sciences, Beijing Institute of Radiation Medicine, Beijing, China

OPEN ACCESS

Edited by:

Praveen K. Dubey,
University of Alabama at Birmingham,
United States

Reviewed by:

Tousif Sultan,
University of Alabama at Birmingham,
United States
Fnu Shiridhar,
University of Central Florida,
United States

*Correspondence:

Dong Han
handong123566@163.com
Feng Cao
fengcao8828@163.com

[†]These authors have contributed
equally to this work and share first
authorship

Specialty section:

This article was submitted to
Cardio-Oncology,
a section of the journal
Frontiers in Cardiovascular Medicine

Received: 05 January 2022

Accepted: 23 February 2022

Published: 23 March 2022

Citation:

Ma Y, Liu X, Bi Y, Wang T, Chen C,
Wang Y, Han D and Cao F (2022)
Alteration of N⁶-Methyladenosine
mRNA Methylation in a Human Stem
Cell-Derived Cardiomyocyte Model of
Tyrosine Kinase Inhibitor-Induced
Cardiotoxicity.
Front. Cardiovasc. Med. 9:849175.
doi: 10.3389/fcvm.2022.849175

Background: N⁶-methyladenosine (m⁶A) plays important roles in various cardiovascular diseases (CVDs), including cardiac hypertrophy and heart failure. Sunitinib (SUN) is a tyrosine kinase inhibitor (TKI) that is widely used in the treatment of different types of solid and blood tumors, but its efficacy is restricted by a concomitant rise in cardiotoxicities. However, the methylation modification of m⁶A messenger RNA (mRNA) in cardiomyocytes treated with TKI has not been investigated.

Methods: The global m⁶A methylation level of SUN-induced cardiotoxicity was detected by m⁶A dot blot and colorimetric methylation assay. MeRIP-Seq (methylated RNA immunoprecipitation sequencing) and RNA-seq (RNA sequencing, input) were employed to depict the landscapes of transcriptome and epitranscriptome in TKI. Changes in major m⁶A-related enzymes were detected by qRT-PCR and Western blot. In addition, the effects of FTO on SUN-induced cardiotoxicity were evaluated by gain and loss of function studies.

Results: In this study, we observed that the m⁶A methylation level was significantly elevated in SUN-treated human-induced pluripotent stem cell-derived cardiomyocytes (hiPSC-CMs) and paralleled a positively correlated cellular damage level. Through a genome-wide analysis of m⁶A mRNA methylation by methylated RNA immunoprecipitation sequencing (MeRIP-seq) and input RNA sequencing (RNA-seq), we identified a total of 2,614 peaks with significant changes, of which 1,695 peaks were significantly upregulated and 919 peaks were significantly downregulated. Quantitative reverse transcription PCR (RT-qPCR), immunofluorescence, and Western blotting revealed that the RNA demethylase fat mass and obesity-associated protein (FTO) was downregulated, whereas the RNA methylases methyltransferase-like 14 (METTL14) and wilms' tumor 1-associating protein (WTAP) were upregulated. Furthermore, gain- and loss-of-function studies substantiated that FTO is cardioprotective in TKI.

Conclusion: This study deciphered the methylation modification of m⁶A mRNA in hiPSC-CMs post-TKI treatment and determined that FTO may be a promising therapeutic target for TKI-induced cardiotoxicity.

Keywords: tyrosine kinase inhibitor (TKI), hiPSC-CMs, N⁶-methyladenosine, FTO, cardiotoxicity

INTRODUCTION

Tyrosine kinase inhibitors (TKIs) have been widely used in the treatment of various types of cancer, some of which are in different stages of clinical development, which shows the importance of tyrosine kinase as the main target of new antitumor drugs (1). However, the widespread use of TKIs was restricted due to their cardiovascular toxicity, which threatened patients' medication compliance and quality of life (2). Therefore, the study of the cardiovascular toxicity mechanism of TKIs is of great significance for circumventing these cardiovascular complications. Sunitinib (SUN), a small-molecule, multitarget receptor tyrosine kinase (RTK) inhibitor, was approved by the US Food and Drug Administration (FDA) in 2006 to treat kidney cancer, gastrointestinal stromal tumors, and endocrine tumors (3). Its targets include vascular endothelial growth factor receptors (VEGFRs), platelet-derived growth factor (PDGFR), and mast/stem cell growth factor receptor (SCFR) (4). In the cardiovascular system, SUN impairs cell signal transduction, cell cycle regulation, and cell metabolism, increasing the incidence of cardiac events in patients with cancer (5). However, cardioprotective strategies based on these mechanisms are controversial and have not been proven in humans, suggesting that SUN-mediated cardiotoxicity may also be mediated by other mechanisms (6).

Ribonucleic acid methylation constitutes more than 60% of all the RNA modifications and N⁶-methyladenosine (m⁶A) is the most prevalent RNA modification in mammalian mRNA and long non-coding RNAs (lncRNAs) (7, 8). The m⁶A modification mainly occurs on adenine in the "RRACH" motif and its state is tightly controlled by "writer" methyltransferases (methyltransferase-like 3 (METTL3), methyltransferase-like 14 (METTL14), and Wilms' tumor 1-associating protein (WTAP)), "eraser" demethylases [fat mass and obesity-associated protein (FTO) and Alk B homologue 5 (ALKBH5)], and "reader" m⁶A binding proteins (YT homology domain containing1 (YTHDC1), YTHDC2, YT homology domain family (YTHDF1), YTHDF2, YTHDF3, heterogeneous nuclear ribonucleo protein C (HNRNPC), heterogeneous nuclear ribonucleoprotein A2B1 (HNRNPA2B1), eukaryotic initiation factor 3A (EIF3A), and EIF3C) (9, 10). Ample evidence suggests that m⁶A modification regulates a variety of RNA metabolic processes, such as mRNA stability, splicing, nuclear transport, and translation capabilities (11–13). Given the importance of m⁶A modification in RNA metabolism, we were, thus, curious to discover whether m⁶A modification had potential effects on TKI-induced cardiotoxicity.

Abbreviations: METTL14, methyltransferase-like 14; WTAP, Wilms' tumor 1-associating protein; ALKBH5, Alk B homologue 5; YTHDF, CYT homology domain family, HNRNPC, heterogeneous nuclear ribonucleo protein C; HNRNPA2B1, heterogeneous nuclear ribonucleoprotein A2B1; EIF3A, eukaryotic initiation factor 3A; RPMI, Roswell Park Memorial Institute; IWR-1, Wnt/β-catenin inhibitor; FB23-2, FTO Demethylase inhibitor; RIPA, Radio-Immunoprecipitation Assay; PVDF, poly vinylidene fluoride; TBST, Tris-Buffered Saline and Tween; ECL, enhanced chemiluminescence; GAPDH, glyceraldehyde-3-phosphate dehydrogenase; DTT, DL-Dithiothreitol; MIT, Massachusetts Institute of Technology; AAV9, adeno-associated virus 9.

Furthermore, previous studies have proposed a cardioprotective role of m⁶A demethylase FTO-mediated demethylating effects in various cardiovascular pathologies. First, reduced FTO expression was observed in failing human hearts and hypoxic cardiomyocytes, thereby increasing m⁶A in RNA and deteriorating cardiomyocyte contractile dysfunction via regulating the methylation of cardiac contractile transcripts (7). Moreover, elevated m⁶A-RNA methylation and FTO repression were causatively involved in myocardial inflammation and dysfunction during endotoxemia in mice (14). Another study showed that FTO overexpression mitigated apoptosis of hypoxia-/reoxygenation-treated myocardial cells by demethylating Mhrt (15). However, the role of FTO in TKI-induced myocardial injury remains to be further revealed.

In this study, we used methylated RNA immunoprecipitation sequencing (MeRIP-seq) and input RNA sequencing (RNA-seq) to study the transcriptome and m⁶A modification epitranscriptome in human-induced pluripotent stem cell-derived cardiomyocytes (hiPSC-CMs) treated with SUN. To gain further insights into the pathological significance of m⁶A modification in TKI-induced cardiotoxicity, the Gene Ontology (GO) and the Kyoto Encyclopedia of Genes and Genomes (KEGG) pathway enrichment analyses were performed on the key genes identified by MeRIP-seq and input RNA-seq. Furthermore, we revealed a cardioprotective role of FTO in SUN-treated hiPSC-CMs. This study is the first study to show that m⁶A methylation may play an indispensable role in TKI-induced cardiotoxicity.

MATERIALS AND METHODS

Cell Culture

Urinary epithelial cell-derived hiPSCs were cultured in Matrigel (Invitrogen, Carlsbad, California, USA)-coated 6-well plates in E8 medium (Invitrogen, Carlsbad, California, USA) containing 0.5% penicillin/streptomycin. HiPSCs were induced to differentiate into cardiomyocytes when cultured at 80% confluence, as previously reported (16, 17). In short, cells were treated with 6 μM of selective inhibition CHIR99021, a selective inhibitor of glycogen synthase kinase 3β, in Roswell Park Memorial Institute (RPMI) medium supplemented with B27 (Invitrogen, Carlsbad, California, USA) for 48 h, followed by 5 μM of Wnt/β-catenin inhibitor (IWR-1), a Wnt antagonist (Sigma-Aldrich), for another 48 h, and the medium was changed every 3 days. On the 10th day, the beating cardiomyocytes were purified by the glucose starvation method for 5 days for further tests.

Isolation and Culture of Cardiac Microvascular Endothelial Cells (CMECs) and Cardiac Fibroblasts (CFs)

Primary CMECs and CFs were isolated, cultured, characterized, and subjected to subsequent experiments, as previously reported (18, 19).

Silence and Overexpression of FTO

We employed commercially available ready-to-use lentiviral constructs pLenti-GIII-CMV (Applied Biological Materials

Incorporation, CAT. NO 210500610196) and FTO small hairpin RNA (shRNA) lentiviral particles (Santa Cruz Biotechnology Incorporation, CAT. NO sc-75002-V) to overexpress or knockdown FTO in hiPSC-CMs. The transfection process was done as per the manufacturer's instructions. Lentivirus particles were transfected at a multiplicity of infection (MOI) of 20.

Cell Viability Assay

Cell viability was detected with a Cell Counting Kit-8 (CCK-8) (C0037, Beyotime, Shanghai, China). The culture medium was aspirated and the precoated Matrigel hiPSC-CMs were washed with phosphate-buffered saline (PBS) once. Then, 100 μ l of working buffer was added to hiPSC-CMs in 96-well plates and the cells were incubated at 37°C for 30 min in the dark. A microplate reader (Tecan, Switzerland) was used to automatically measure the absorbance at a wavelength of 450 nm.

Drug Treatment

Our preliminary results showed that the half-maximal inhibitory concentration (IC₅₀) of SUN treatment for 24 h (cell viability serving as the readout) is around 6 μ M (**Supplementary Figure S1A**); thus, the subsequent experiments were carried out with 6 μ M SUN (SU11248, Selleck, Shanghai, China) treatment for 24 h and equal volume of dimethyl sulfoxide (DMSO) treatment for 24 h served as the control group. For FTO Demethylase inhibitor (FB23-2) (S8837, Selleck, Shanghai, China) treatment, 20 μ M FB23-2 was added simultaneously with SUN for 24 h. The concentration of FB23-2 was chosen based on a previous report (20).

Western Blot Analysis

Cell protein was extracted with Radio-Immunoprecipitation Assay (RIPA) Lysis Solution (P0013C, Beyotime, Shanghai, China) from hiPSC-CMs for Western blot detection. Protein extractions and molecular weight standards were separated by 10% sodium dodecyl sulfate-polyacrylamide gel electrophoresis (SDS-PAGE) gels and transferred to poly vinylidene fluoride (PVDF) membranes (Bio-Rad, USA). After blocking, the membrane was incubated with primary antibodies [methyltransferase-like 3, (METTL3) ab195352, Abcam; METTL14, ab220030, Abcam; FTO, ab126605, Abcam; ALKBH5 aa302-330, LifeSpan Biosciences; WTAP, 56501, Cell Signaling Technology; and glyceraldehyde-3-phosphate dehydrogenase (GAPDH) ab8245, Abcam] at 4°C overnight in a 5% bovine serum albumin (BSA) blocking solution. After being washed with Tris-Buffered Saline and Tween (TBST) buffer, the membrane was incubated in 5% blocking buffer for 1 h at room temperature with the secondary antibody (1:800 dilution, 7074, Cell Signaling Technology, USA) at the recommended dilution. Protein bands were detected with the enhanced chemiluminescence (ECL) chemiluminescent kit (P0018S, Beyotime, Shanghai, China) in a dark room and assessed with Image Lab software (Bio-Rad, USA).

N⁶-Methyladenosine Dot Blot

The mRNA was isolated with the Dynabeads[®] mRNA Purification Kit (61006, Invitrogen, Carlsbad, California,

USA) and the purity of mRNA was detected by the NanoDrop method for further tests. The serially diluted mRNA was denatured at a high temperature of 95°C and cooled immediately after denaturation. The 2 μ l sample was transferred directly onto a nucleic acid-optimized nylon membrane (1620153, Bio-Rad, USA). After a regimen UV cross-linking and methylene blue (M4591, Sigma-Aldrich, USA) staining, the membrane was blocked by soaking in 5% BSA buffer and incubated with the anti-m⁶A antibody (ab284130, Abcam, Shanghai, China) in 5% BSA for 30 min at room temperature. Then, the membrane was incubated with horseradish peroxidase (HRP)-conjugated secondary antibody (ab97051, Abcam, Shanghai, China) for 30 min, followed by incubation with the ECL reagent (P0018S, Beyotime, Shanghai, China) for 1 min, covered with plastic wrap, and exposed to different lengths of exposure in a dark room. The test sample was compared with the signal of the standard sample to detect its concentration.

m⁶A RNA Methylation Assay (Colorimetric)

The m⁶A RNA Methylation Assay Kit (ab185912, Abcam, Shanghai, China) was used to measure the m⁶A level of mRNA. According to the instructions, 80 μ l of binding solution was added to each well and negative control, diluted positive control, and 200 ng of mRNA were added to each well and incubated at 37°C for 90 min. Fifty microliter of diluted capture antibody was added for incubation at room temperature for 60 min and then 50 μ l of diluted detection antibody was added to each well for 30 min. Finally, 100 μ l of developing solution was used for the reaction and after incubation in the dark at room temperature for 10 min, stop solution was added and the absorbance was measured at 450 nm.

Lactate Dehydrogenase (LDH) Release

The LDH Release Detection Kit (C0016, Beyotime, Shanghai, China) was used to detect cell cytotoxicity according to the instructions. Sixty microliter of LDH detection working solution was added to each well. The sample was incubated at room temperature (~25°C) in the dark for 30 min. Then, the absorbance was measured at 490 nm.

Quantitative Reverse Transcription PCR (RT-qPCR)

Total RNA was extracted from hiPSC-CMs using the RNAsimple Total RNA Kit (DP419, Tiangen, Beijing, China). One microgram of total RNA was used for complementary DNA (cDNA) synthesis reaction, as previously described (21). The isolated mRNA was reverse transcribed into cDNA with the High Capacity cDNA Reverse Transcription Kit (4368814, Invitrogen, Carlsbad, California, USA) and cDNA was amplified with the Takara's Perfect Real-Time PCR Kit (RR037A, Takara Bio, Otsu, Japan). The primers and probes were ordered from TaqMan (Invitrogen, Carlsbad, California, USA). The relative level of each mRNA was quantified by GAPDH and expressed as a relative ratio.

Methylated RNA Immunoprecipitation Sequencing

Guangzhou Epibiotek Corporation Ltd. (Guangzhou, China) provided the MeRIP-seq service. Briefly, m⁶A RNA immunoprecipitation was performed with the GenSeq™ m⁶A RNA IP Kit (GE-ET-001, GenSeq Incorporation, China) according to the manufacturer's instructions. Both the input samples were obtained by ribosomal RNA (rRNA) removal and smart principles and first-strand cDNA PCR-enriched library fragments were synthesized. The magnetic bead library fragments were purified by DNA and the ultrafine RNA methylated m⁶A detection library was obtained. The library quality was evaluated using the Bioptic Qsep100 Analyzer (Agilent Technologies Incorporation, USA). Library sequencing was performed on an Illumina HiSeq instrument in PE150 sequencing mode.

Methylated RNA Immunoprecipitation Sequencing Data Processing

Cutadapt (version 2.5) was used to trim adapters and filter for sequences. The remaining reads were then aligned to the human Ensemble genome GRCh38 (mouse Ensemble genome GRCm38) using Hisat2 aligner (version 2.1.0) under the following parameters: “-rna-strandness RF.” m⁶A peaks were identified using the exome Peak R package (version 2.13.2) under the parameter: “peak_cutoff_p-value = 0.05, peak_cutoff_false discovery rate (FDR) = NA, and fragment_length = 200.”

Differential m⁶A peaks were identified using the exome Peak R package under the following parameters: “peak_cutoff_p-value = 0.05, peak_cutoff_FDR = NA, and fragment_length = 200.” The GO and the KEGG analyses were performed using the cluster profile R package (version 3.6.0). m⁶A RNA-related genomic features were visualized using the Guitar R package (version 1.16.0). Identified m⁶A peaks with p-values < 0.05 were chosen for the *de-novo* motif analysis using homer (version 4.10.4) under the parameter “-len 6-rna.”

Long RNA-seq

The Epi™ Mini LongRNA-SEQ Kit (E1802, Epibiotek, Guangzhou, China) and the Epi™ DNA Clean Beads Kit (R1809, Epibiotek, Guangzhou, China) was used for long RNA sequencing. DNase I was added to the RNA samples and digested at 37°C for 30 min to remove the residual DNA in the samples and the RNA was purified and recovered by magnetic beads. rRNA removal and RNA fragmentation: 5XRT buffer was added to sample RNA, a rRNA probe, and a temperature gradient reaction was used to fragment RNA samples and remove rRNA. Synthesis of first-strand cDNA: EpiScript™ IV, RNase inhibitor, DL-Dithiothreitol (DTT), Template-Switching oligonucleotide (TSO), and random primers were added to the RNA samples in Step 2. After mixing with the wall of the tube, rapid centrifugation was carried out in the PCR machine according to the following procedures: 37°C, 90 min; 70°C, 15 min. 2XpfuMax HiFi PCR ProMix and sequencing primers were added to the first-strand cDNA samples and then amplified in a PCR apparatus after mixing. The Epi™ DNA Clean Beads were used to purify PCR products in a 1X ratio. DNA fragments (300–400 bp) were recovered from the purified products with magnetic beads in a 0.65/0.2X ratio for a second round of PCR amplification to enrich

300–400 bp DNA fragments. The Bioptic Qsep100 Analyzer was used to conduct quality inspection of the library to detect whether the size distribution of the library conformed to the theoretical size.

Ribonucleic Acid Sequencing Data Processing

Cutadapt (version 2.5) was used to trim adapters and filter for sequences and the remaining reads were then aligned to the human Ensemble genome GRCh38 (mouse Ensemble genome GRCm38) using Hisat2 aligner (version 2.1.0) under the parameter “-rna-strandness RF.” The reads mapping the genome were calculated using feature counts (version 1.6.3). Differential gene expression analysis was performed using the DESeq2 R package. Enrichment analysis was performed using the clusterProfiler R package for the GO terms and the KEGG database pathways.

Immunostaining and Immunofluorescence Analysis

Human-induced pluripotent stem cell-derived cardiomyocytes were separated and placed in 6-well plates (Corning, New York, USA). The combined staining of α -actinin (ab137346, Abcam), immunoglobulin G (IgG) H&L (Alexa Fluor® 488) (ab150077, Abcam), and propidium iodide (PI) 1 μ g/ml (ST511, Beyotime, Shanghai, China) was used to detect cardiomyocyte death. The nucleus was stained with 4',6-diamidino-2-phenylindole (DAPI) (C1002, Beyotime, Shanghai China) and the dead cells were labeled with PI to pass through the damaged cell membrane. A Nikon A1R HD25 confocal microscope was used to capture images. The total number of cells in the PI-positive and five randomly selected fields was counted using ImageJ software by a researcher blinded to the treatment assignments. A manual pipeline (CellProfiler, Broad Institute of Massachusetts Institute of Technology (MIT) and Harvard in Cambridge) was used to determine the cell surface area (22). Briefly, 5 to 6 random pictures were taken with 20X magnification and 150–200 cells/per condition were analyzed in order to determine cell size following the instructions of the software.

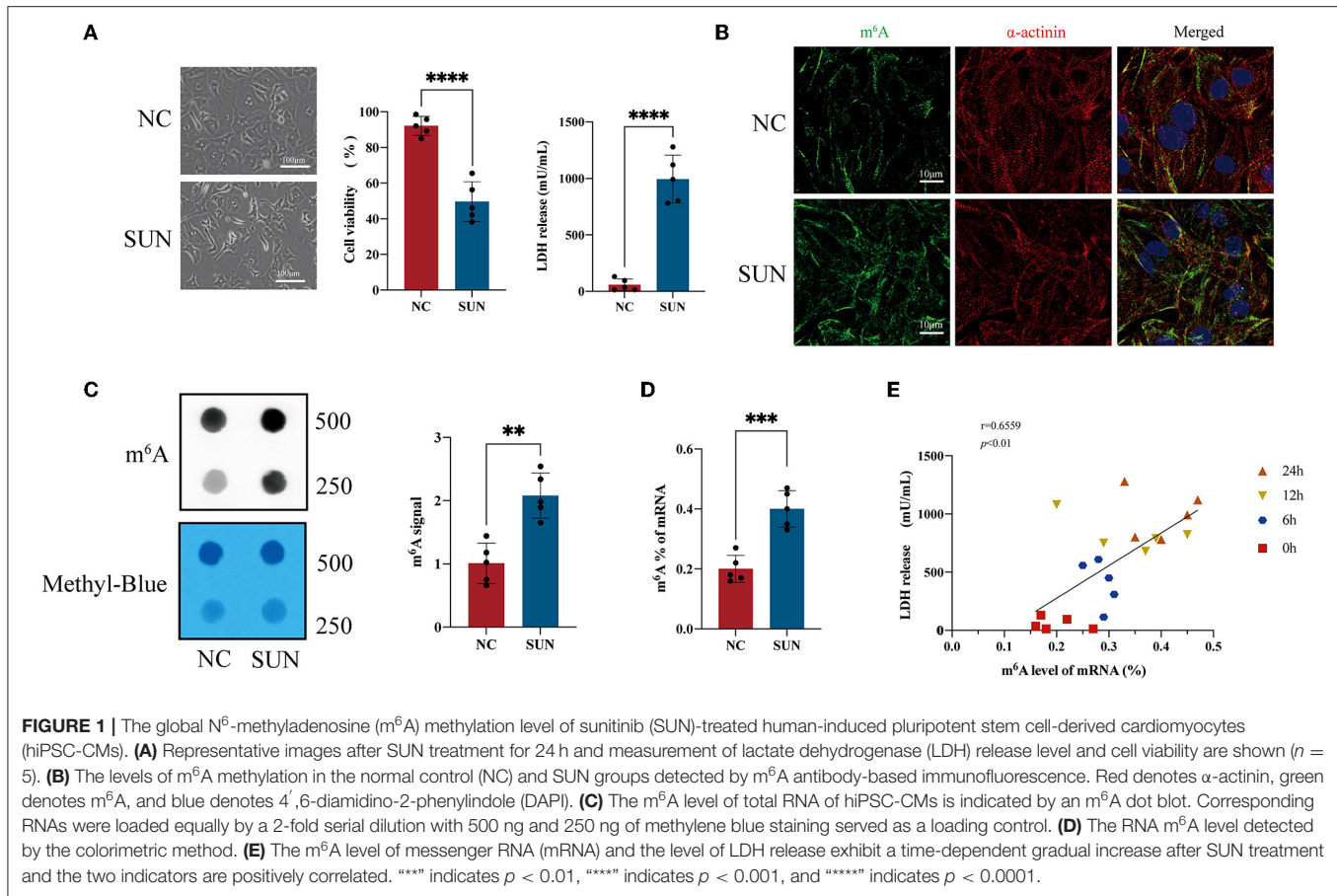
Statistical Analyses

Continuous data are expressed as the mean \pm SD unless otherwise specified. Comparisons between the two or more groups were performed using the Student's *t*-test and ANOVA for normal variables or the Mann-Whitney *U* test and the Kruskal-Wallis test for non-normal variables. R software (version 3.4.2) and GraphPad Prism software (version 8.00) were used for statistical analysis. Biological replicates (individual mice) are shown as individual data points superimposed on bar charts. Significance was conventionally accepted at *p* < 0.05.

RESULTS

Global m⁶A Level Was Upregulated in SUN-Injured hiPSC-CMs

The treatment dose and duration of SUN were determined based on preliminary experiments. Our preliminary results showed that the IC₅₀ of SUN treatment for 24 h



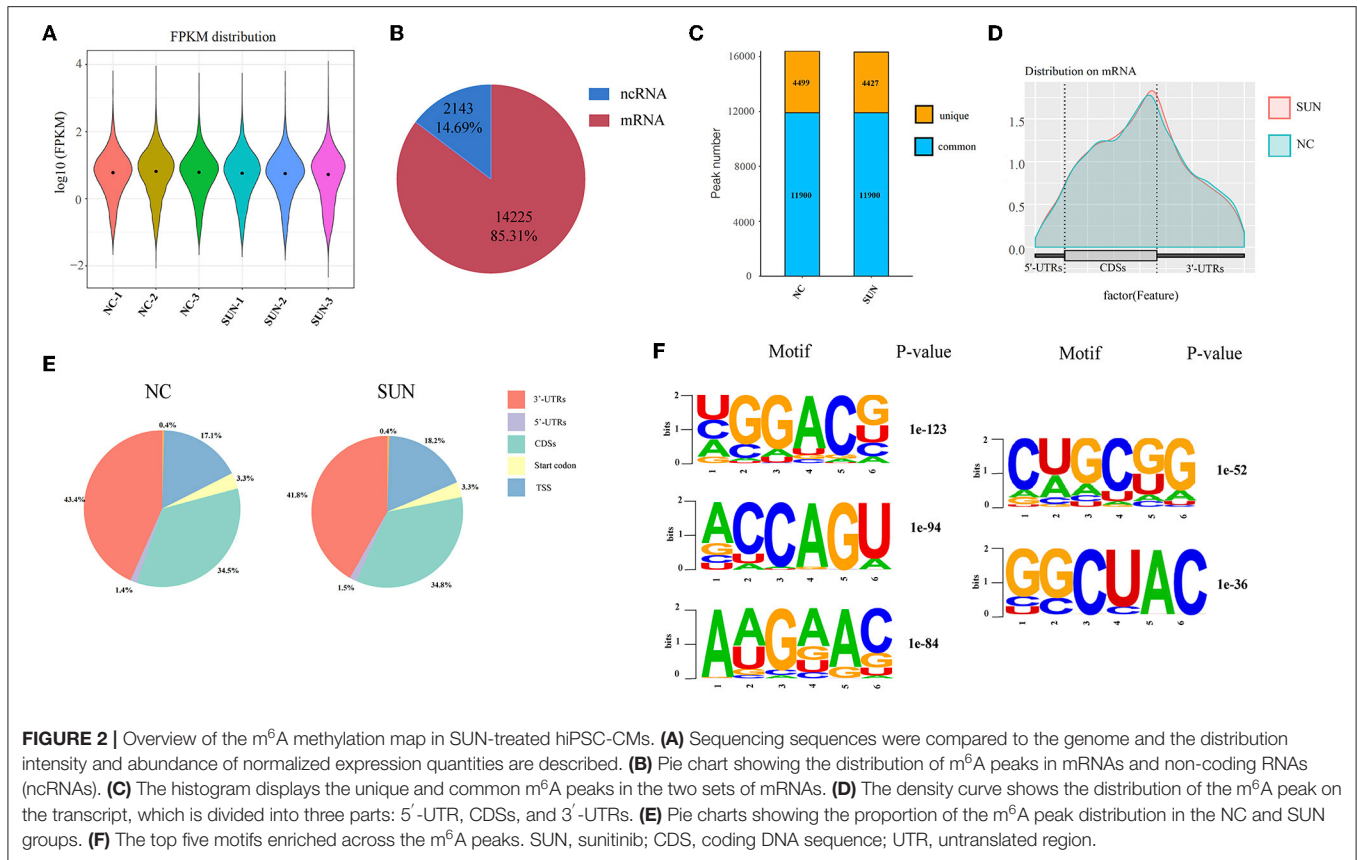
(cell viability serving as the readout) is around $6\mu\text{M}$ (**Supplementary Figure S1A**); thus, the subsequent experiments were carried out with $6\mu\text{M}$ SUN treatment for 24 h and equal volume of DMSO treatment for 24 h served as the control group. Furthermore, we also explored the time kinetics of $6\mu\text{M}$ SUN in hiPSC-CMs; these results were given in **Supplementary Figure S1B**.

Figure 1A shows the optical microscope morphology of hiPSC-CMs treated with $6\mu\text{M}$ of SUN for 24 h. The cell surface area decreased, accompanied by a significant elevation in LDH release and a significant reduction in cell viability in SUN-treated hiPSC-CMs. Furthermore, the immunofluorescence results suggested that the global m⁶A levels in the SUN group increased and that the structure of myocardial sarcomeres became disorganized (**Figure 1B**). The m⁶A dot blot validated that the global m⁶A level was indeed elevated in the SUN group (**Figure 1C**). In addition, the colorimetric kit method also verified the upregulation of the global m⁶A level (**Figure 1D**). Linear regression was used to analyze the relationship between the mRNA m⁶A level and LDH release of hiPSC-CMs after SUN treatment and it was found that a positive correlation was identified between the global m⁶A level and LDH release ($r = 0.6096$, $p < 0.01$) and the global m⁶A level and LDH release gradually increased as the treatment time was prolonged (**Figure 1E**). Overall, these results

indicated that the dysregulated m⁶A modification in SUN-injured hiPSC-CMs may play important roles in TKI-induced cardiotoxicity.

Overview of the m⁶A Methylation Map in SUN-Injured hiPSC-CMs

Next, to further decipher the role of elevated m⁶A in SUN-injured hiPSC-CMs, three biological copies of hiPSC-CMs from either the normal control (NC) group or the SUN group were sent for MeRIP-seq and m⁶A MeRIP enrichment regions (peaks) were analyzed after sample normalization (**Figure 2A**). The m⁶A modification mostly occurred in mRNAs (**Figure 2B**). A total of 16,399 m⁶A peaks from 4,499 coding gene transcripts (mRNAs) were identified in the NC group. In the SUN group, there were 16,732 m⁶A peaks within 4,427 mRNAs (**Figure 2C**). To reveal the preferential distribution of m⁶A in transcripts, the metagene profiles of all the identified m⁶A peaks in the entire transcriptome were probed. The results show that the m⁶A peak is preferentially enriched in two sets of coding DNA sequences (CDSs) and the 3'-untranslated region (UTR) (**Figures 2D,E**). To learn whether a consensus motif existed in the identified m⁶A peaks, we used HOMER software to map the m⁶A methylation. The results showed that m⁶A mainly exists in the consensus sequence of 5'-RRAH-3' and 5'-RRAH-3' (R = A or G; H = A, C, or U) (14). Among the identified m⁶A peaks, the top five conserved

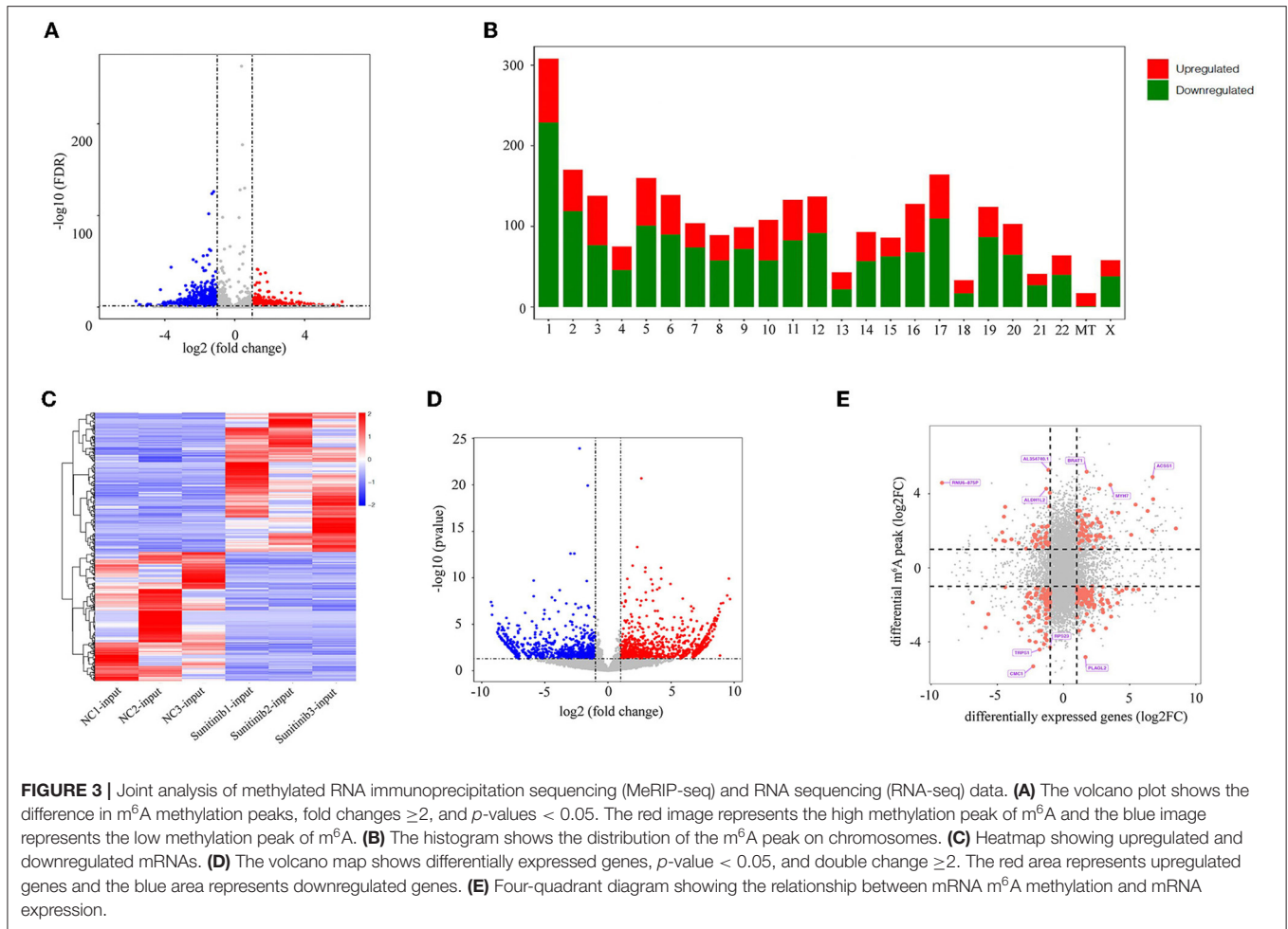


motifs are shown in **Figure 2F**, which was consistent with the well-known “RRACH” consensus motif of m⁶A modification.

Conjoint Analysis of the MeRIP-seq and RNA-seq Data in SUN-Injured hiPSC-CMs

To further clarify the changes in m⁶A methylation associated with TKI-induced cardiotoxicity, we performed a conjoint analysis of the MeRIP-seq and RNA-seq data. As shown in **Figure 3A**, 20,072 m⁶A peaks (representing 9,892 genes) were identified and there were 2,614 differentially methylated peaks (representing 2,066 genes), among which 919 differentially methylated peaks had hypermethylation and 1,695 differentially methylated peaks had hypomethylation at the log fold change cutoff of (± 1) and FDR cutoff of < 0.05 . The top 10 hypermethylated genes and the top 10 hypomethylated genes are shown in **Table 1**. The analysis of the differentially methylated peak (DMPeaks) distribution at different chromosome loci revealed that the chromosomes with the most m⁶A methylation were chromosome 1 with 308 m⁶A methylation peaks, chromosome 2 with 170 m⁶A methylation peaks, and chromosome 17 with 164 m⁶A methylation peaks (**Figure 3B**). In parallel, RNA-seq was used to determine the transcriptome profile of altered genes. We identified 1,906 differentially expressed genes (DEGs) between the NC and SUN groups, including 990 upregulated DEGs and 916 downregulated DEGs (fold changes 2, $p < 0.05$;

Figures 3C,D). The top 10 upregulated mRNAs and the top 10 downregulated mRNAs are shown in **Table 2**. Furthermore, among the 20,072 m⁶A peaks (representing 9,892 genes) identified, there were 2,614 differentially methylated peaks (representing 2,066 genes), 919 hypermethylated peaks, and 1,695 hypomethylated peaks. Accordingly, we identified 244 mRNAs with significant changes in their m⁶A peaks and levels and they could be divided into four quadrants: both the mRNA expression and m⁶A peaks were upregulated (55), mRNA and m⁶A peaks were both downregulated (74), m⁶A peaks were upregulated and mRNA peaks were downregulated (37), and m⁶A peaks were downregulated and mRNA peaks were upregulated (78) (**Figure 3E**). We have validated the transcriptomic study by examining the gene expression level of top 5 upregulated and top 5 downregulated protein coding genes among the 244 intersection genes by RT-qPCR assay. The RT-qPCR results were mostly consistent with RNA-seq (**Supplementary Figure S2**), which might be helpful to solidify our sequencing result. The list of 244 DEGs with significant differential m⁶A peaks is given in **Supplementary Table S2**. Their GO term for enrichment analysis is given in **Supplementary Figure S3**. The GO analysis showed that the biological functions of the 244 mRNAs were mainly enriched in mitogen-activated protein kinase (MAPK) and p53 signaling pathway, while the KEGG analysis repetitiously pointed to apoptotic signaling pathways.



The GO and the KEGG Enrichment Analyses Revealed the Biological Information Underlying DEGs and Differentially Methylated Genes (DMGs)

To explore the physiological and pathological significance of the DEGs and DMGs, the GO and the KEGG pathway analyses were performed on the key genes identified. The GO analysis showed that the biological functions of upregulated DEGs were mainly enriched in the regulation of angiogenesis and apoptosis signaling pathways (Figure 4A). The downregulated DEGs were mainly involved in microtubule cytoskeleton organization, endomembrane system organization, protein tetramerization, and protein heterodimerization (Figure 4B). Through the KEGG analysis, the upregulated DEGs were mainly enriched in pathways in cell adhesion molecules (CAMs), extracellular matrix (ECM)-receptor interaction, and ribosome biogenesis in eukaryotes (Figure 4C). The downregulated DEGs were mainly involved in cancer pathways, the MAPK signaling pathway, cytokine-cytokine receptor interactions, and the p53 signaling pathway (Figure 4D). In addition, we also performed enrichment analyses on DMGs. These genes were mainly enriched in pathways such as nuclear transport, nucleocytoplasmic transport,

regulation of cell cycle phase transition, and histone modification (Figure 4E). The KEGG analyses showed that these DMGs were related to pathways in cancer, focal adhesion, regulation of actin cytoskeleton, and protein processing in the endoplasmic reticulum (Figure 4F).

Expression of FTO Was Downregulated, While the Expressions of MELLT14 and ALKBH5 Were Upregulated in SUN-Treated hiPSC-CMs

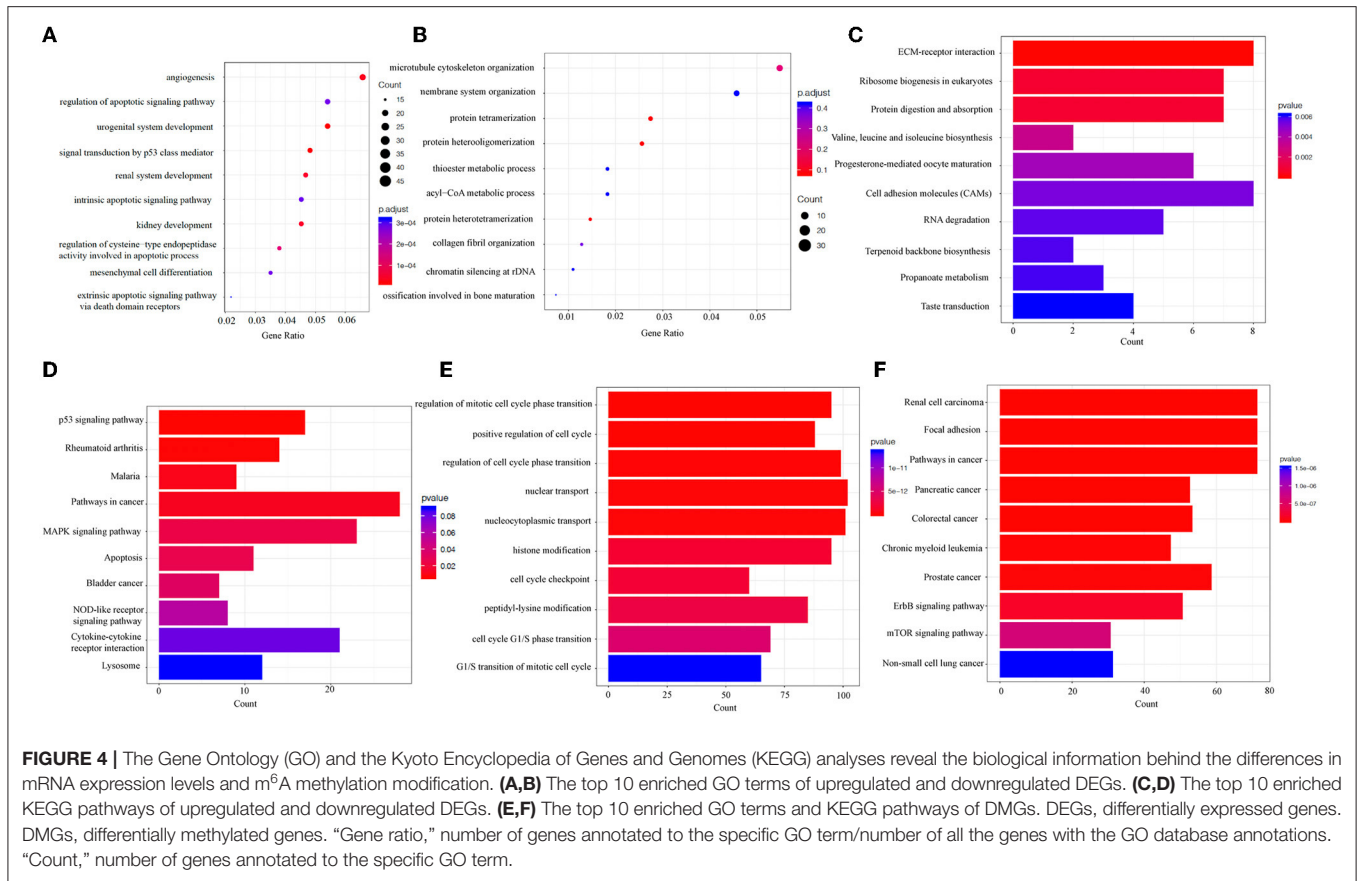
To further explore whether the m⁶A modification enzyme was involved in SUN-induced hiPSC-CM injury, we examined the expression levels of major methyltransferases and demethylases. Compared with the NC group, the mRNA expression levels of the methylases WTAP and METTL14 in the SUN group were significantly upregulated ($p < 0.05$), whereas the mRNA expression level of FTO (demethylase) was significantly downregulated in the SUN group ($p < 0.01$) (Figure 5A). The downregulation of FTO was again verified in the SUN group by immunofluorescence (IF) staining (Figure 5B). However, the expression of the other two enzymes, METTL3 and ALKBH5, was not altered in SUN-treated hiPSC-CMs. Consistent with the

TABLE 1 | List of the top 10 hypomethylated genes and the top 10 hypermethylated genes.

Genes	Description	Chromosome	Peak start	Peak end	log ₂ Fold change	P-value	Up/down
FAM69B	Family with sequence similarity 69 member B	9	136,723,693	136,724,020	-5.65	1.023e-8	Down
ATXN1	Ataxin 1	6	16,300,520	16,300,791	-5.46	1.58e-4	Down
SLC30A6	Solute carrier family 30 member 6	2	32,224,109	32,224,289	-5.39	4.07e-4	Down
JAM2	Junctional adhesion molecule 2	21	25,716,872	25,717,262	-5.04	0.0036	Down
NRDE2	Nuclear RNAi defective 2	14	90,270,343	90,270,584	-5.02	3.31e-4	Down
MANEL	Mannosidase like protein	1	37,799,732	37,800,181	-4.98	5.89e-5	Down
PLAGL2	Pleiomorphiccad-enomagene like 2	20	32,195,399	32,195,639	-4.82	7.41e-5	Down
TRPS1	Trichorhinophalangeal syndrome type 1	8	115,412,594	115,412,805	-4.42	0.0024	Down
TSPAN5	Tetraspanin 5	4	98,472,253	98,472,524	-4.33	0.0013	Down
RPS23	Ribosomal protein S23	5	82,275,563	82,275,772	-4.29	0.0043	Down
RGMB	Repulsive guidance molecules B	5	98,795,779	98,796,079	6.15	4.47e-8	Up
TTN	Titin	2	178,693,982	178,702,575	5.98	0.0035	Up
NEBL	Nebulette	10	20,831,577	20,845,420	5.89	0.0010	Up
FABP3	Fat acid binding protein 3	1	31,369,427	31,372,984	5.64	1.70e-4	Up
STOX2	Stork head box 2	4	184,009,557	184,009,768	4.98	0.0051	Up
DYRK3	Dual-specificity tyrosine-(Y)-phosphorylation regulated kinase 3	1	206,647,569	206,647,839	4.94	0.0054	Up
BRAT1	Breast cancer type 1 associated ring domain 1	7	2,542,069	2,542,339	4.83	1.15e-4	Up
ZNF697	Zinc finger protein 697	1	119,624,014	119,625,981	4.52	1.82e-5	Up
LSM14A	RNA-associated protein 55A,	19	34,228,887	34,229,157	4.49	1.70e-5	Up
CCDC184	Coiled-coil domain containing 184	12	48,184,769	48,185,096	4.44	4.57e-4	Up

TABLE 2 | List of the top 10 upregulated messenger RNAs (mRNAs) and the top 10 downregulated mRNAs.

Description	log ₂ Fold change	P-value	Up/down	
CATSPER2	The cation channel of sperm receptor 2	-9.1720856	1.01E-07	Down
ITGB7	Integrin Beta 7	-8.6837258	3.99E-05	Down
CLDN20	Claudin 20	-8.6824254	8.49E-06	Down
GMPR	Guanosine monophosphate reductase	-8.6137908	0.00021296	Down
USP50	Ubiquitin-specific peptidase 50	-8.5858481	9.24E-06	Down
PCDHA7	Protocadherin alpha 7	-8.402541	0.00040126	Down
ZP1	Zona pellucida glycoprotein 1	-8.3886407	0.00054659	Down
SLC37A4	Glucose-6-phosphate transporter member 4	-8.3131318	2.82E-05	Down
KCNC1	Potassium voltage-gated channel 1	-8.2366521	0.00065662	Down
LPAR4	Lysophosphatidic acid receptor 4	-8.1447607	0.00105897	Down
PGF	Vascular endothelial growth factor	9.66737242	2.05E-08	Up
AVP11	Arginine vasopressin-induced 1	9.44284665	8.06E-09	Up
ANKRD45	Ankyrin repeat domain 45	9.11522806	5.18E-08	Up
TNFRSF10A	Tumor necrosis factor receptor superfamily member 10A	8.94685039	5.80E-08	Up
MYOCD	Myocardin	8.87253755	0.02317118	Up
NPTX1	Neuronal pentraxin 1	8.84367054	4.82E-07	Up
SLCO4A1	Solute carrier organic anion transporter family, member 4A1	8.77762835	2.14E-07	Up
MEDAG	Mesenteric estrogen-dependent adipogenesis protein	8.60841757	2.70E-06	Up
IGSF9	Immunoglobulin superfamily, member 9	8.51141356	1.63E-05	Up
SULT1C2	Sulfotransferase family, cytosolic 2C	8.49784929	2.13E-06	Up



mRNA expression data, the protein levels of WTAP, METTL14, and FTO exhibited similar trends in SUN-treated hiPSC-CMs (**Figure 5C**). Collectively, these results indicated that the downregulated FTO as well as the upregulated METTL14 and WTAP might account for the increased global m⁶A level in SUN-injured hiPSC-CMs.

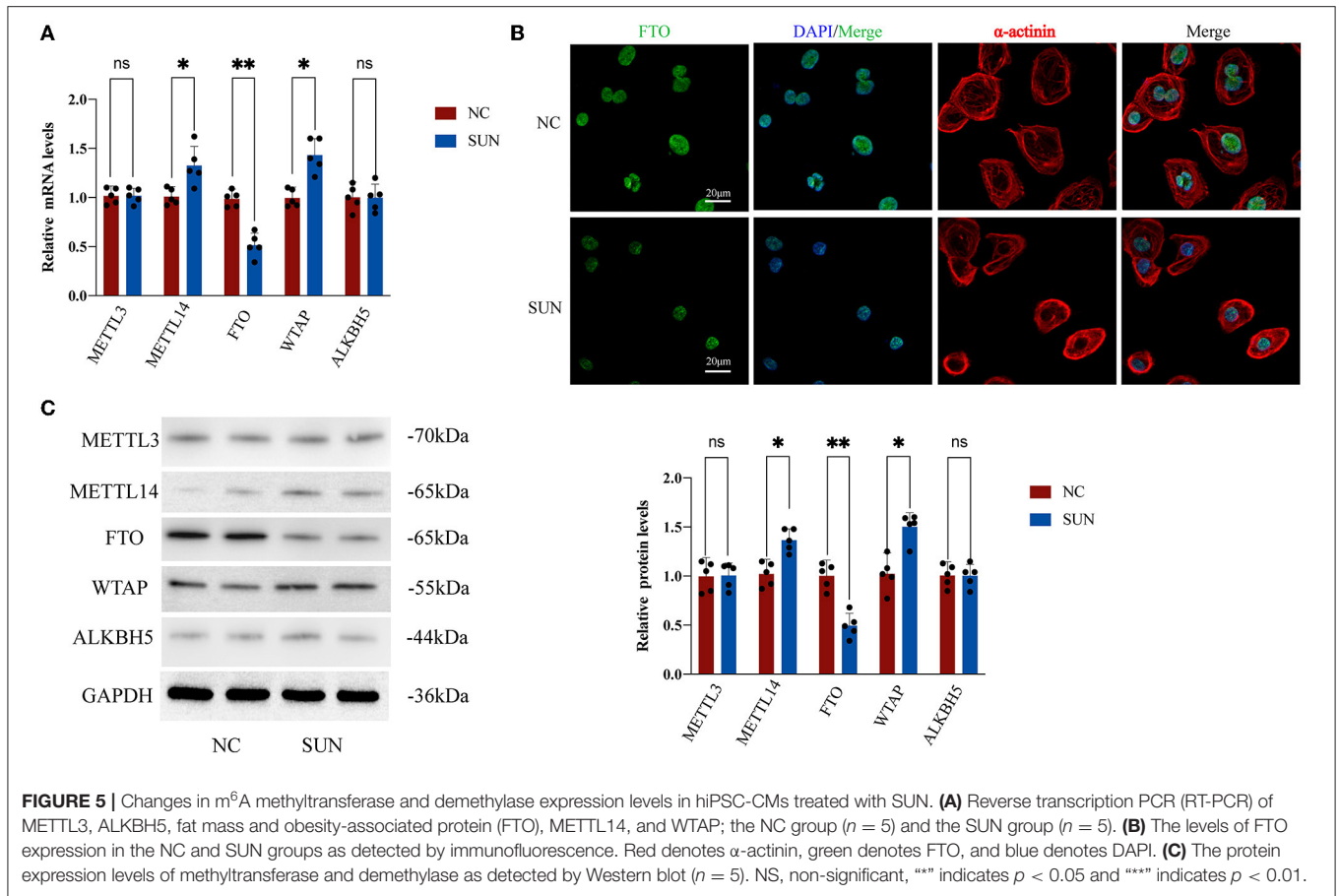
FTO Downregulation Aggravated SUN-Induced hiPSC-CM Injury

Next, we employed FB23-2, a potent and selective FTO inhibitor that directly binds to FTO and selectively inhibits FTOs m⁶A demethylase activity to examine the role of FTO in SUN-induced hiPSC-CM injury. For FB23-2 treatment, 20 μM FB23-2 was added simultaneously with SUN for 24 h. The concentration of FB23-2 was chosen based on a previous report (20). We examined the effect of FB23-2 on global m⁶A level by m⁶A dot blot. The results verified a ~1.7-fold upregulation of global m⁶A level. Cell death was evaluated by PI staining after 24 h of treatment. Interestingly, SUN-induced hiPSC-CM death was exacerbated in the FB23-2 + SUN group (**Figures 6A,B**). This effect was not observed in normal hiPSC-CMs, indicating that FB23-2 alone would not affect the cell viability of hiPSC-CMs. Furthermore, SUN-induced hiPSC-CM atrophy was also aggravated in the FB23-2 + SUN group, as evidenced by a smaller cell surface area (**Figures 6A,C**). The colorimetric test kit for LDH release again validated the findings obtained from the PI

staining (**Figure 6D**). In addition, we knocked down FTO using a FTO shRNA lentiviral particles. The silencing efficiency and inhibited FTO activity as revealed by elevated global m⁶A level were confirmed (**Supplementary Figures S6A,B**). We observed that FTO shRNA phenocopied the effects of FTO inhibitor in terms of elevating PI-positive cell death, LDH release, and reducing cell surface area (**Figures 6A–D**). Taken together, these results indicate that FTO plays a protective role in SUN-induced hiPSC-CM injury.

To further explore the role of FTO in SUN-induced cardiotoxicity, we employed a lentivirus construct to overexpress FTO. After verifying the FTO mRNA and global m⁶A level, we transfected hiPSC-CMs with the FTO lentivirus construct or empty vector. The results showed that FTO overexpression by lentivirus construct successfully induced a ~2-fold upregulation of FTO expression and a ~40% downregulation of global m⁶A level (**Supplementary Figures S5A,B**). Furthermore, FTO overexpression significantly reduced LDH release and improved cell viability in SUN-challenged hiPSC-CMs (**Supplementary Figures S5C,D**).

To justify that SUN-altered m⁶A effects are cardiomyocytes specific or not, we treated CMECs and CFs with 60 nM or 10 μM SUN for 18 h, respectively, referring to the concentration and duration reported in previous studies (23, 24). We then measured the global m⁶A level of mRNA and the transcripts levels of FTO mRNA. Interestingly enough, both the CMECs and



CFs failed to show significant changes in these two parameters in response to SUN (**Supplementary Figures S7A,B,D,E**). Furthermore, cotreatment of FTO inhibitor FB23-2 did not alter the reduced cell viability in response to SUN as revealed by CCK-8 assay (**Supplementary Figures S7C,F**). These results might indicate that the reported effects are cardiomyocytes specific.

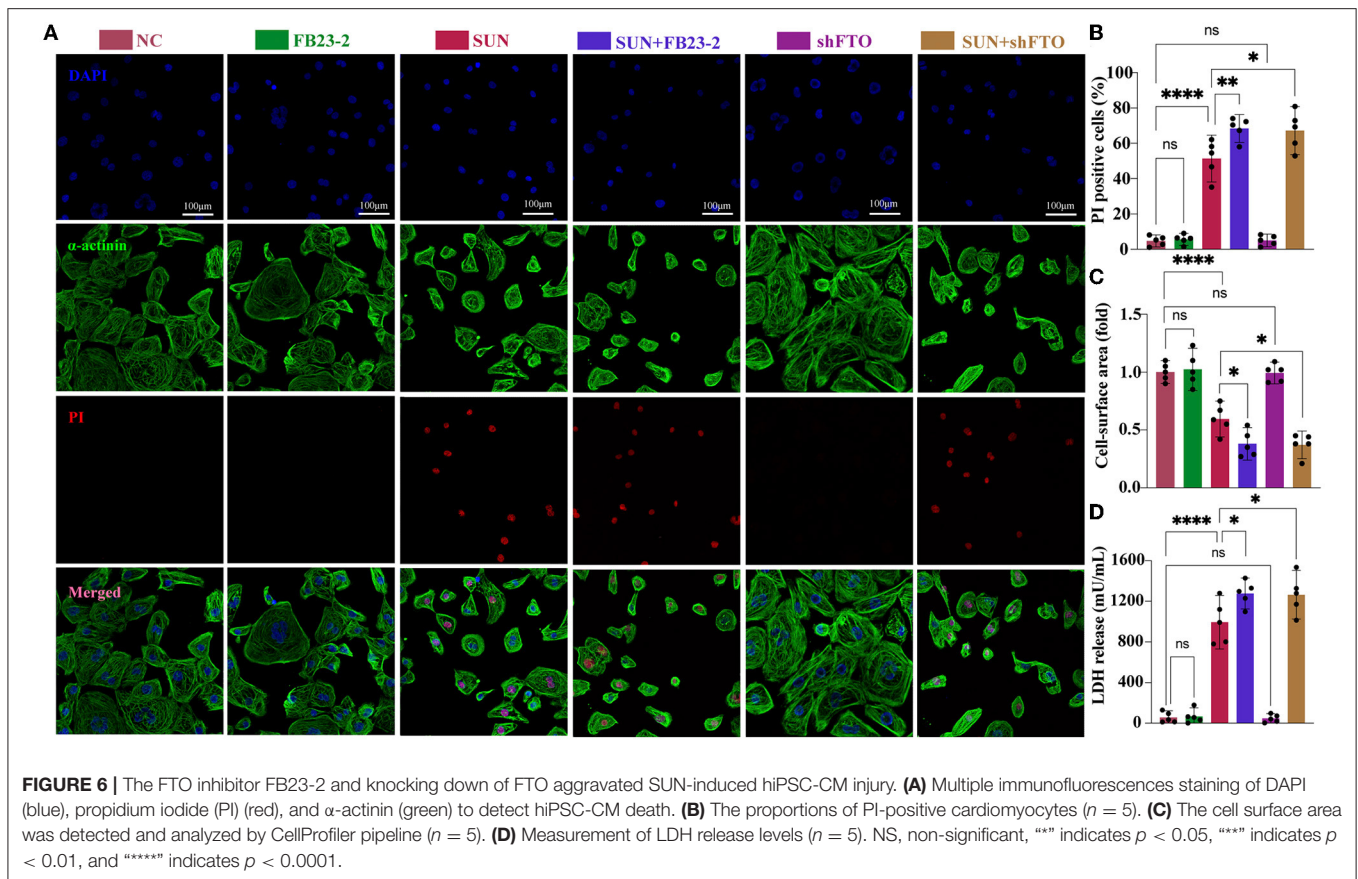
DISCUSSION

In this study, we performed a genome-wide analysis of m⁶A mRNA methylation by MeRIP-seq and RNA-seq in a human stem cell-derived cardiomyocyte model of TKI-induced cardiotoxicity. Our major findings include the following: (a) the global m⁶A level was upregulated in SUN-injured hiPSC-CMs; (b) downregulated FTO as well as upregulated METTL14 and WTAP might account for the increased global m⁶A level in SUN-injured hiPSC-CMs; (c) m⁶A modification was associated with the occurrence and course of TKI-induced cardiotoxicity to some extent; and (d) protected against SUN-induced hiPSC-CM injury. Nevertheless, the specific mechanism of m⁶A methylation in TKI-induced cardiotoxicity remains to be further studied in the future.

Recent studies have shown that m⁶A is involved in the occurrence and development of cancers and cardiac

dysfunction. RNA methyltransferases, demethylases, and m⁶A-binding proteins are frequently altered in human cancer tissues from various organ sources, influencing cancer transcription and oncoprotein expression, cancer cell proliferation, survival, tumor initiation, progression, and metastasis (25, 26). However, there is no consensus on whether altered m⁶A is oncogenic or tumor suppressive. In comparison, studies have reported that m⁶A methylation and FTO have decreased expressions in various pathologic conditions including heart failure and endotoxemia- and hypoxia-/reoxygenation-induced cardiac cell injuries (7, 14, 15). In accordance with our present finding, most studies suggest that elevated m⁶A level that result from elevated methylases or reduced demethylases is a deleterious factor for the onset and progression of various cardiovascular diseases (27).

Recently, m⁶A methylation was revealed to play important roles in various cardiovascular diseases, but its role in TKI-induced cardiotoxicity has rarely been studied. In this study, we found that the cell viability of hiPSC-CMs treated with SUN decreased, whereas the release of LDH increased, which suggested that SUN had a damaging effect on hiPSC-CMs. IF staining showed that the m⁶A levels of the SUN group were elevated and the m⁶A dot blot also verified this elevation. Moreover, we also found that the global m⁶A methylation level in SUN-treated hiPSC-CMs was positively correlated with LDH release. Therefore, we employed MeRIP-seq and RNA-seq to



study the transcriptome and methylome in SUN-treated hiPSC-CMs. Through further joint analysis of MeRIP-seq and RNA-seq data, we found significant differences between the m⁶A methylation and mRNA expression levels of 244 genes. We surmised that these potential genes, through m⁶A methylation, are potentially involved in the occurrence and development of TKI-induced cardiotoxicity.

We further conducted the GO and the KEGG analyses of differentially expressed m⁶A methylated genes. Biological processes and pathways indicated apoptotic signaling pathways that were repetitiously enriched by upregulated DEGs. This enrichment pattern coincides with previous SUN cardiotoxicity studies. For instance, a previous study in isolated cardiomyocytes and mice scrutinized the potential mechanisms of SUN-associated cardiac effects. This study concluded that mitochondrial injury and cardiomyocyte apoptosis accounted for SUN-associated cardiotoxicity (28). In a more recent report, apoptotic cell death resulting from mitochondrial damage with reactive oxygen species (ROS) accumulation was shown to be the important contributing mechanism of cardiotoxicity associated with SUN (29). Conversely, thioester and acetyl-CoA metabolic pathways were significantly enriched by downregulated DEGs. Thioesters play a prominent role in metabolism. The central metabolite acetyl-CoA is a thioester that is produced mainly by oxidative decarboxylation of pyruvate or by fatty acid degradation. It is, thus, possible that SUN-induced cardiotoxicity can be ascribed to interrupted mitochondrial energy production.

Interestingly, SUN was previously reported to induce loss of mitochondrial membrane potential and energy rundown in cardiomyocytes (30). Thus, this study further supports the notion that apoptosis induction and energy reduction are the crucial mechanisms of SUN-associated cardiotoxicity.

Fat mass and obesity-associated protein is the first demethylase discovered to be involved in m⁶A modification. Recent high-quality studies have confirmed that FTO plays fundamental roles in many cardiac physiological and pathological processes. Increased m⁶A in RNA was associated with decreased FTO mRNA and protein expression in human and mouse failing hearts. Moreover, adeno-associated virus 9 (AAV9)-mediated myocardial FTO overexpression restores cardiac function in mouse models of myocardial infarction, whereas cardiomyocyte-restricted knockout of FTO mice deteriorates cardiac function (27). Further mechanistic studies revealed that FTO overexpression selectively demethylates cardiac contractile transcripts, thus blocking their degradation and improving their stability and expression under ischemia, which eventually contributed to reduced fibrosis and enhanced angiogenesis (7). Another study found that FTO alleviated cardiac dysfunction by regulating glucose uptake and glycolysis in mice with pressure overload-induced heart failure, the effects of which were associated with demethylation of the glycolysis-related gene *Pgam2* (31). In addition, a similar study reported that FTO cardiomyocyte-specific knockout worsened cardiac dysfunction through transcription-independent mechanisms

of translation regulation (32). All these reports support a cardioprotective role of FTO in different cardiac pathologies. In this study, we detected the major methylases and demethylases in SUN-treated hiPSC-CMs and found that FTO was significantly downregulated. To verify the role of FTO in SUN-induced cardiotoxicity, we treated hiPSC-CMs with FB23-2, a potent and selective FTO inhibitor and demonstrated that FB23-2 can aggravate the cell injury elicited by SUN, cause damage to the sarcomeres of cardiomyocytes, and deteriorate cell atrophy. Together with previous findings, this study might add a conceptual framework for targeting FTO as a therapeutic for various cardiovascular diseases. Notably, this study also found that the expression levels of METTL14 and WTAP increased in SUN-treated hiPSC-CMs and their functional roles remain to be further clarified.

This study failed to reveal the downstream regulatory mechanisms by which SUN-stimulated m⁶A upregulation regulates the mRNA expression of related genes, which warrants further investigations. Nonetheless, we have depicted the m⁶A modification landscape of SUN-treated hiPSC-CMs with transcriptome-wide unbiased epitranscriptomics and revealed a potential role of m⁶A and m⁶A eraser FTO in SUN-induced cardiotoxicity, which would lay a solid foundation for further detailed mechanistic studies.

CONCLUSION

This study provides the first overview of the m⁶A methylation map in SUN-injured hiPSC-CMs to decipher the RNA post-transcriptional epigenetic mechanisms of TKI-induced cardiotoxicity. Through MeRIP-seq, we found that the m⁶A methylation level in 2,614 mRNAs changed significantly. Combined analysis of the m⁶A peak and mRNA expression showed that 244 mRNAs were significantly changed after SUN treatment. These genes with varying levels of m⁶A modification may play an important role in the process of TKI-induced cardiotoxicity. In addition, we found that inhibiting FTO can aggravate the myocardial toxicity caused by SUN, which suggests a novel therapeutic target for TKI-induced cardiotoxicity.

REFERENCES

1. Thomas A, Rajan A, Giaccone G. Tyrosine kinase inhibitors in lung cancer. *Hematol Oncol Clin North Am.* (2012) 26:589–605. doi: 10.1016/j.hoc.2012.02.001
2. Moslehi JJ, Deininger M. Tyrosine kinase inhibitor-associated cardiovascular toxicity in chronic myeloid leukemia. *J Clin Oncol.* (2015) 33:4210–8. doi: 10.1200/JCO.2015.62.4718
3. Bex A, Mulders P, Jewett M, Wagstaff J, van Thienen JV, Blank CU, et al. Comparison of immediate vs deferred cytoreductive nephrectomy in patients with synchronous metastatic renal cell carcinoma receiving sunitinib: the SURTIME randomized clinical trial. *JAMA Oncol.* (2019) 5:164270. doi: 10.1001/jamaoncol.2018.5543
4. Ferrari SM, Centanni M, Virili C, Miccoli M, Ferrari P, Ruffilli I, et al. Sunitinib in the treatment of thyroid cancer. *Curr Med Chem.* (2019) 26:963272. doi: 10.2174/0929867324666171006165942
5. Chintalgattu V, Rees ML, Culver JC, Goel A, Jiffar T, Zhang J, et al. Coronary microvascular pericytes are the cellular target of

DATA AVAILABILITY STATEMENT

The data presented in the study are deposited in the NCBI Gene Expression Omnibus (GEO) database repository, accession number GSE192913.

AUTHOR CONTRIBUTIONS

FC and DH conceived and designed the experiments, provided financial support, co-wrote the article, and edited the manuscript. YM and XL performed the experiments. YM, XL, YB, TW, CC, and YW analyzed the data. All authors contributed to the article and approved the submitted version.

FUNDING

This study was supported by the National Natural Science Foundation of China (82100372, 81820108019, and 91939303), the Innovative Project of Chinese PLA General Hospital (CX19028), the Key Health Care Projects of National Health Commission (2020ZD05), National Postdoctoral Program for Innovative Talents (BX20200154), Beijing Nova Program (Z211100002121048), and the Basic Research Reinforcement Project (2021-JCJQ-JJ-1079).

ACKNOWLEDGMENTS

We acknowledge Jie Zhou for valuable comments on data analysis, Yanfei Zhang for assistance on the generation and amplification of cDNA templates.

SUPPLEMENTARY MATERIAL

The Supplementary Material for this article can be found online at: <https://www.frontiersin.org/articles/10.3389/fcvm.2022.849175/full#supplementary-material>

- sunitinib malate-induced cardiotoxicity. *Sci Transl Med.* (2013) 5:187ra69. doi: 10.1126/scitranslmed.3005066
6. Yang Y, Bu P. Progress on the cardiotoxicity of sunitinib: prognostic significance, mechanism and protective therapies. *Chem Biol Interact.* (2016) 257:125:31. doi: 10.1016/j.cbi.2016.08.006
7. Mathiyalagan P, Adamiak M, Mayourian J, Sassi Y, Liang Y, Agarwal N, et al. FTO-dependent N-methyladenosine regulates cardiac function during remodeling and repair. *Circulation.* (2019) 139:518:32. doi: 10.1161/CIRCULATIONAHA.118.033794
8. Liu Z-X, Li L-M, Sun H-L, Liu S-M. Link between m⁶A modification and cancers. *Front Bioeng Biotechnol.* (2018) 6:89. doi: 10.3389/fbioe.2018.00089
9. Meyer KD, Patil DP, Zhou J, Zinoviev A, Skabkin MA, Elemento O, et al. 5' UTR m⁶A promotes cap-independent translation. *Cell.* (2015) 163:999–1010. doi: 10.1016/j.cell.2015.10.012
10. Gao R, Ye M, Liu B, Wei M, Ma D, Dong K. m⁶A modification: a double-edged sword in tumor development. *Front Oncol.* (2021) 11:679367. doi: 10.3389/fonc.2021.679367

11. Tang Y, Chen K, Song B, Ma J, Wu X, Xu Q, et al. m⁶A-Atlas: a comprehensive knowledgebase for unraveling the N⁶-methyladenosine (m⁶A) epitranscriptome. *Nucleic Acids Res.* (2021) 49:D134–43. doi: 10.1093/nar/gkaa692
12. Li Y, Gu J, Xu F, Zhu Q, Chen Y, Ge D, Lu C. Molecular characterization, biological function, tumor microenvironment association and clinical significance of m⁶A regulators in lung adenocarcinoma. *Brief Bioinform.* (2021) 22:bbaa225. doi: 10.1093/bib/bbaa225
13. Chen X-Y, Zhang J, Zhu J-S. The role of m⁶A RNA methylation in human cancer. *Mol Cancer.* (2019) 18:18:103. doi: 10.1186/s12943-019-1033-z
14. Dubey PK, Patil M, Singh S, Dubey S, Ahuja P, Verma SK, Krishnamurthy P. Increased m⁶A-RNA methylation and FTO suppression is associated with myocardial inflammation and dysfunction during endotoxemia in mice. *Mol Cell Biochem.* (2021) 477:129–41. doi: 10.1007/s11010-021-04267-z
15. Shen W, Li H, Su H, Chen K, Yan J. FTO overexpression inhibits apoptosis of hypoxia/reoxygenation-treated myocardial cells by regulating m⁶A modification of Mhrt. *Mol Cell Biochem.* (2021) 476:2171–9. doi: 10.1007/s11010-021-04069-6
16. Han D, Wang Y, Wang Y, Dai X, Zhou T, Chen J, et al. The tumor-suppressive human circular RNA CircITCH sponges miR-330-5p to ameliorate doxorubicin-induced cardiotoxicity through upregulating SIRT6, survivin, and SERCA2a. *Circ Res.* (2020) 127:e108–25. doi: 10.1161/CIRCRESAHA.119.316061
17. Qiu Y, Ma Y, Jiang M, Li S, Zhang J, Chen H, et al. Melatonin alleviates LPS-induced pyroptotic cell death in human stem cell-derived cardiomyocytes by activating autophagy. *Stem Cells Int.* (2021) 2021:8120403. doi: 10.1155/2021/8120403
18. Wang D, Luo P, Wang Y, Li W, Wang C, Sun D, et al. Glucagon-like peptide-1 protects against cardiac microvascular injury in diabetes via a cAMP/PKA/Rho-dependent mechanism. *Diabetes.* (2013) 62:1697–708. doi: 10.2337/db12-1025
19. Li X, Han D, Tian Z, Gao B, Fan M, Li C, et al. Activation of cannabinoid receptor type II by AM1241 ameliorates myocardial fibrosis via Nrf2-mediated inhibition of TGF- β 1 pathway in myocardial infarction mice. *Cell Physiol Biochem.* (2016) 39:1521–36. doi: 10.1159/000447855
20. Zhao T, Wang J, Wu Y, Han L, Chen J, Wei Y, et al. Increased m⁶A modification of RNA methylation related to the inhibition of demethylase FTO contributes to MEHP-induced Leydig cell injury. *Environ Pollut.* (2021) 268:115627. doi: 10.1016/j.envpol.2020.115627
21. Han D, Wang Y, Chen J, Zhang J, Yu P, Zhang R, et al. Activation of melatonin receptor 2 but not melatonin receptor 1 mediates melatonin-conferred cardioprotection against myocardial ischemia/reperfusion injury. *J Pineal Res.* (2019) 67:e12571. doi: 10.1111/jpi.12571
22. Carpenter AE, Jones TR, Lamprecht MR, Clarke C, Kang IH, Friman O, et al. CellProfiler: image analysis software for identifying and quantifying cell phenotypes. *Genome Biol.* (2006) 7:R100. doi: 10.1186/gb-2006-7-10-r100
23. Chiusa M, Hool S-L, Truetsch P, Djafarzadeh S, Jakob SM, Seifriz F, et al. Cancer therapy modulates VEGF signaling and viability in adult rat cardiac microvascular endothelial cells and cardiomyocytes. *J Mol Cell Cardiol.* (2012) 52:1164–75. doi: 10.1016/j.yjmcc.2012.01.022
24. McMullen CJ, Chalmers S, Wood R, Cunningham MR, Currie S. Sunitinib and imatinib display differential cardiotoxicity in adult rat cardiac fibroblasts that involves a role for calcium/calmodulin dependent protein kinase II. *Front Cardiovasc Med.* (2020) 7:630480. doi: 10.3389/fcvm.2020.630480
25. Lan Q, Liu PY, Haase J, Bell JL, Hüttelmaier S, Liu T. The critical role of RNA m⁶A methylation in cancer. *Cancer Res.* (2019) 79:1285–92. doi: 10.1158/0008-5472.CAN-18-2965
26. Ma S, Chen C, Ji X, Liu J, Zhou Q, Wang G, et al. The interplay between m⁶A RNA methylation and noncoding RNA in cancer. *J Hematol Oncol.* (2019) 12:121. doi: 10.1186/s13045-019-0805-7
27. Wu S, Zhang S, Wu X, Zhou X. m⁶A RNA methylation in cardiovascular diseases. *Mol Ther.* (2020) 28:2111–9. doi: 10.1016/j.ymthe.2020.08.010
28. Chu TF, Rupnick MA, Kerkela R, Dallabrida SM, Zurakowski D, Nguyen L, et al. Cardiotoxicity associated with tyrosine kinase inhibitor sunitinib. *Lancet.* (2007) 370:2011–19. doi: 10.1016/S0140-6736(07)61865-0
29. Bouitbir J, Alshaiqhi A, Panajatovic MV, Abegg VF, Paech F, Krähenbühl S. Mitochondrial oxidative stress plays a critical role in the cardiotoxicity of sunitinib: running title: sunitinib and oxidative stress in hearts. *Toxicology.* (2019) 426:152281. doi: 10.1016/j.tox.2019.152281
30. Kerkela R, Woulfe KC, Durand J-B, Vagnozzi R, Kramer D, Chu TF, et al. Sunitinib-induced cardiotoxicity is mediated by off-target inhibition of AMP-activated protein kinase. *Clin Transl Sci.* (2009) 2:15(20). doi: 10.1111/j.1752-8062.2008.00090.x
31. Zhang B, Jiang H, Wu J, Cai Y, Dong Z, Zhao Y, et al. m⁶A demethylase FTO attenuates cardiac dysfunction by regulating glucose uptake and glycolysis in mice with pressure overload-induced heart failure. *Signal Transduct Target Ther.* (2021) 6:377. doi: 10.1038/s41392-021-00699-w
32. Berulava T, Buchholz E, Elerdashvili V, Pena T, Islam MR, Lbik D, et al. Changes in m⁶A RNA methylation contribute to heart failure progression by modulating translation. *Eur J Heart Fail.* (2020) 22:54:20. doi: 10.1002/ehf.1672

Conflict of Interest: The authors declare that the research was conducted in the absence of any commercial or financial relationships that could be construed as a potential conflict of interest.

Publisher's Note: All claims expressed in this article are solely those of the authors and do not necessarily represent those of their affiliated organizations, or those of the publisher, the editors and the reviewers. Any product that may be evaluated in this article, or claim that may be made by its manufacturer, is not guaranteed or endorsed by the publisher.

Copyright © 2022 Ma, Liu, Bi, Wang, Chen, Wang, Han and Cao. This is an open-access article distributed under the terms of the Creative Commons Attribution License (CC BY). The use, distribution or reproduction in other forums is permitted, provided the original author(s) and the copyright owner(s) are credited and that the original publication in this journal is cited, in accordance with accepted academic practice. No use, distribution or reproduction is permitted which does not comply with these terms.